



# Prospects for Measuring $H \rightarrow$ invisible at the FCCee

Aman Desai <sup>1,\*</sup> and Paul Jackson <sup>1,†</sup>

<sup>1</sup>*Department of Physics, Adelaide University, North Terrace, Adelaide, SA 5005, Australia*

(Dated: May 14, 2026)

We present the prospects for measuring  $H \rightarrow$  invisible decays at the Future Circular Collider electron-positron at  $\sqrt{s} = 240$  GeV with an integrated luminosity of  $10.8 \text{ ab}^{-1}$ . In this study, we consider the  $ZH$  production mode with three decay modes of the  $Z$  boson:  $Z \rightarrow e^+e^-$ ,  $Z \rightarrow \mu^+\mu^-$  and  $Z \rightarrow jj$  ( $b\bar{b}, c\bar{c}, s\bar{s}, q\bar{q}$ ). We find that at 95% confidence limit, the combined upper limit on the  $\mathcal{B}(H \rightarrow \text{invisible})$  could reach 0.15%.

## I. INTRODUCTION

In the Standard Model of particle physics (SM) the Higgs boson can decay invisibly via  $H \rightarrow ZZ \rightarrow \nu\bar{\nu}\nu\bar{\nu}$  with a branching fraction of 0.106% [1]. The ATLAS and CMS collaborations have investigated this decay channel and have reported upper limits on the branching fraction [2, 3].

The Future Circular Collider-ee (FCC-ee) is a proposed electron-positron collider to be built at CERN [4]. This collider facility aims to explore interactions across a centre-of-mass energy range extending from the  $Z$  mass (91 GeV) and reaching up to the top quark pair production threshold (365 GeV). Among the centre-of-mass energies,  $\sqrt{s} = 240$  GeV is crucial for investigating the Higgs boson owing to the high cross-section for the primary production process  $ZH$  at this energy [5]. At these energies and with an expected integrated luminosity of  $10.8 \text{ ab}^{-1}$ , it is expected that the FCC-ee will produce  $\sim 2.2 \times 10^6$  Higgs boson. This would allow precision measurements of several Higgs decay modes along with the Higgs boson's total decay width. At the FCC-ee, at  $\sqrt{s} = 240$  GeV, we expect to see  $\sim 10^3$  invisibly decaying Higgs boson.

Previous studies investigating the  $\mathcal{B}(H \rightarrow \text{invisible})$  channel have been carried out in the context of the proposed lepton colliders such as the CEPC [6], CLIC [7], ILC [8] as well as the FCC-ee [9], among others.

We analyze the  $e^+e^- \rightarrow ZH$  process considering the  $Z$  boson decays:  $Z \rightarrow qq, ee, \mu\mu$  and the Higgs boson decaying invisibly. We use multivariate analysis methods to discriminate the signal from background in addition to

using a set of selection criteria.

This paper is organized as follows: We discuss the Monte Carlo simulation in Section II; in Section III we present the analysis procedure and the statistical inference is presented in Section IV.

## II. EVENT SIMULATION

In this analysis, we use Monte Carlo samples prepared centrally by the FCC-ee as part of the WINTER2023 Campaign [10]. The signal process in this analysis is the production mode:  $e^+e^- \rightarrow ZH$  with  $Z$  boson decaying either to a pair of electrons/muons or quarks and the Higgs boson decaying invisibly. The invisible decays of the Higgs boson are simulated via the process  $H \rightarrow ZZ \rightarrow \nu\bar{\nu}\nu\bar{\nu}$ . Therefore, there are three different signals which are analyzed:  $Z(ee)H(\text{inv})$ ,  $Z(\mu\mu)H(\text{inv})$  and  $Z(qq)H(\text{inv})$ . The list of signal processes used in this analysis and their cross-sections are given in Table I.

Physics processes that mimic the signal or have the potential to do so are considered as backgrounds. In particular, the backgrounds differ in each of the  $Z$  decay channel. The set of backgrounds for three analysis is given in Table II along with the corresponding cross-section and number of events simulated for analysis.

The simulation of all backgrounds except  $ZZ$ ,  $Z(qq)$  and  $WW$  is carried out using WHIZARD3 [11] followed by parton shower and hadronisation implemented in PYTHIA6 [12]. The  $ZZ$ ,  $Z(qq)$ , and  $WW$  backgrounds are generated via PYTHIA8 [13]. All the simulated events are processed through the parametric response of the proposed IDEA detector [14] achieved through its implementation within the DELPHES software [15]. The simulations have also implemented initial state radiation, final state radiation and a gaussian beam spread.

\* aman.desai@adelaide.edu.au

† p.jackson@adelaide.edu.au

TABLE I: Signal processes considered at  $\sqrt{s} = 240$  GeV along with the number of generated events and cross-sections [10].

Process	$N_{\text{events}}$	Cross-section [fb]	Channel
$e^+e^- \rightarrow e^+e^-H(\rightarrow ZZ)$ Inv.	$1.20 \times 10^6$	$7.52 \times 10^{-3}$	$ee$
$e^+e^- \rightarrow \mu^+\mu^-H(\rightarrow ZZ)$ Inv.	$1.20 \times 10^6$	$7.10 \times 10^{-3}$	$\mu\mu$
$e^+e^- \rightarrow qqH(\rightarrow ZZ)$ Inv.	$1.20 \times 10^6$	$5.60 \times 10^{-2}$	$jj$
$e^+e^- \rightarrow bbH(\rightarrow ZZ)$ Inv.	$1.172 \times 10^6$	$3.15 \times 10^{-2}$	$jj$
$e^+e^- \rightarrow ccH(\rightarrow ZZ)$ Inv.	$1.20 \times 10^6$	$2.45 \times 10^{-2}$	$jj$
$e^+e^- \rightarrow ssH(\rightarrow ZZ)$ Inv.	$1.20 \times 10^6$	$3.15 \times 10^{-2}$	$jj$

TABLE II: Background processes considered at  $\sqrt{s} = 240$  GeV along with the number of generated events and cross-sections [10].

Process	$N_{\text{events}}$	Cross-section [fb]	Channel
$e^+e^- \rightarrow ZZ$	$5.62 \times 10^7$	$1.36 \times 10^3$	$ee, \mu\mu, jj$
$e^+e^- \rightarrow W^+W^-$	$3.73 \times 10^8$	$1.64 \times 10^4$	$ee, \mu\mu, jj$
$e^+e^- \rightarrow \nu\bar{\nu}H(\rightarrow ZZ)$ No Inv.	$1.20 \times 10^6$	1.17	$ee, \mu\mu, jj$
$e^+e^- \rightarrow \nu\bar{\nu}H(\rightarrow WW)$	$1.20 \times 10^6$	9.94	$ee, \mu\mu, jj$
$e^+e^- \rightarrow \nu\bar{\nu}Z$	$2.00 \times 10^6$	33.2	$ee, \mu\mu, jj$
$e^+e^- \rightarrow Z/\gamma^* \rightarrow e^+e^-$	$5.34 \times 10^7$	$5.28 \times 10^3$	$ee$
$e^+e^- \rightarrow e^+e^-H(\rightarrow ZZ)$ No Inv.	$1.20 \times 10^6$	0.18	$ee$
$e^+e^- \rightarrow Z/\gamma^* \rightarrow \mu^+\mu^-$	$8.54 \times 10^7$	$8.35 \times 10^3$	$\mu\mu$
$e^+e^- \rightarrow \mu^+\mu^-H(\rightarrow ZZ)$ No Inv.	$1.20 \times 10^6$	0.17	$\mu\mu$
$e^+e^- \rightarrow \nu\bar{\nu}H(\rightarrow \mu\mu)$	$4.0 \times 10^5$	0.01	$\mu\mu$
$e^+e^- \rightarrow Z/\gamma^* \rightarrow q\bar{q}$	$1.01 \times 10^8$	$5.26 \times 10^4$	$jj$
$e^+e^- \rightarrow qqH(\rightarrow ZZ)$ No Inv.	$1.20 \times 10^6$	1.35	$jj$
$e^+e^- \rightarrow bbH(\rightarrow ZZ)$ No Inv.	$1.20 \times 10^6$	0.76	$jj$
$e^+e^- \rightarrow ccH(\rightarrow ZZ)$ No Inv.	$1.20 \times 10^6$	0.59	$jj$
$e^+e^- \rightarrow ssH(\rightarrow ZZ)$ No Inv.	$1.20 \times 10^6$	0.76	$jj$
$e^+e^- \rightarrow \nu\bar{\nu}H(\rightarrow bb)$	$1.20 \times 10^6$	26.7	$jj$
$e^+e^- \rightarrow \nu\bar{\nu}H(\rightarrow cc)$	$1.20 \times 10^6$	1.34	$jj$
$e^+e^- \rightarrow \nu\bar{\nu}H(\rightarrow ss)$	$1.20 \times 10^6$	$1.1 \times 10^{-2}$	$jj$
$e^+e^- \rightarrow qqH(\rightarrow WW)$	$1.10 \times 10^6$	11.5	$jj$
$e^+e^- \rightarrow bbH(\rightarrow WW)$	$1.00 \times 10^6$	6.45	$jj$
$e^+e^- \rightarrow ccH(\rightarrow WW)$	$1.20 \times 10^6$	5.02	$jj$
$e^+e^- \rightarrow ssH(\rightarrow WW)$	$1.20 \times 10^6$	6.45	$jj$

A right-handed coordinate system is defined with its origin at the collision point. The  $x$ -axis points toward the center of the FCC-ee collider, the  $y$ -axis is oriented vertically upward, and the  $z$ -axis is aligned along the beam direction. Azimuthal angles are measured from the  $x$ -axis, while polar angles are defined relative to the  $z$ -axis. For the IDEA detector simulation, electrons and muons

with transverse momentum  $p_T > 100$  MeV and pseudorapidity  $|\eta| < 2.56$  are assumed to be fully reconstructed with 100% efficiency. After accounting for detector effects, including material-induced scattering, the identification efficiency for electrons and muons with energy  $E > 2$  GeV and  $|\eta| < 3$  is assumed to be 99%.

The exclusive Durham  $k_T$  algorithm implemented in

the FASTJET software [16–20] is used for jet clustering. Here, the distance between two particles is given by:

$$d_{ij} = 2 \min(E_i^2, E_j^2)(1 - \cos \theta_{ij}) \quad (1)$$

Prior to jet clustering, the hard electrons or muons are removed from the list of physics objects passed on to the jet clustering stage. The  $N_{\text{jet}}$  parameter of the algorithm is set to two, hence reclustering objects entering the algorithm into two jets in the final state. We have used the  $E$ -recombination scheme. This algorithm also gives one access to variables such the  $d_{23}, d_{34}$  variables which are useful in discriminating events consistent with the two jets hypothesis versus events that may contain more jets but are reclustered as two jets.

The Event generation and simulation software chain have been implemented within the KEY4HEP software [21] stack.

### III. ANALYSIS

The analysis is carried out in the FCCANALYSES software framework [22]. In this section we discuss the analysis which we implemented in three orthogonal channels according to the decay mode of the  $Z$  boson. In particular, we consider the decay modes with  $Z$  boson decaying leptonically to electrons or muons and hadronic decays. The orthogonalization of the subanalyses is achieved at the preselection stage. In particular, for analysis with final states consisting of electrons (muons), we require exactly two electrons (muons) and zero muons (electrons) with their momenta  $p > 5$  GeV. Additionally, the sum of charges is required to be zero. For the hadronic final states, the events are chosen such that the final states consisting of two jets constructed using the exclusive Durham  $k_T$  algorithm as described in the previous section are chosen with zero electrons or muons with  $p > 5$  GeV. Owing to the nature of invisible Higgs decay, we preselect events with missing momenta  $p^{\text{miss}} > 5$  GeV. Moreover, in the case of final state consisting of jets, we require  $\sqrt{d_{23}} < 60$  GeV as well as  $\sqrt{d_{34}} < 40$  GeV. The kinematic distributions for the final states after preselection stage are given in [Figure 1](#) for  $Z(ee)H(\text{inv.})$ , [Figure 2](#) for  $Z(\mu\mu)H(\text{inv.})$ , and [Figure 3](#) for  $Z(jj)H(\text{inv.})$ .

In each of the following sub-analyses, the  $Z$  boson is reconstructed using its visible decay products. As we re-

quire the presence of exactly two electrons (muons) in the case of leptonically decaying  $Z$  boson and since we have two jets in hadronic final state owing to the configuration of the jet clustering algorithm, the reconstruction procedure is simplified. The recoil mass of Higgs boson is computed using the visible decay products of the  $Z$  boson. The recoil mass is defined as:

$$M_{\text{Recoil}} = s + m_Z^2 - 2E_z\sqrt{s} \quad (2)$$

This reconstruction of variables is followed by a selection-based analysis. The selection criteria applied to the events is independent of the final states and is as follows. Firstly, we restrict the  $Z$  boson mass to lie within [87, 95] GeV. This ensures that events such as the ones coming from  $WW$  background are suppressed. In order to veto events not consisting the Higgs boson, we impose requirement on the recoil mass such that it satisfies  $120 \text{ GeV} < m_{\text{recoil}} < 130 \text{ GeV}$ . This selection removes most of the events coming from  $ZZ$ , and from  $Z \rightarrow f\bar{f}$  ( $f$  can be a lepton or jet). The presence of neutrinos in the final state leads to signatures of missing four-momenta and angles of the missing momenta vector. The restriction is imposed on  $|\cos \theta_{\text{miss}}| < 0.95$ . In particular,  $|\cos \theta_{\text{miss}}|$  variable allows us to veto a significant fraction of events coming from  $Z \rightarrow f\bar{f}$ .

For imposing each selection criteria we compute the significance achieved. This quantity is defined as  $Z = S\sqrt{S+B}$  where  $S, B$  represent the Signal and Background yield. The cutflow tables are presented in [Table III](#) for  $Z(ee)H(\text{inv.})$ , [Table IV](#) for  $Z(\mu\mu)H(\text{inv.})$ , and [Table V](#) for  $Z(jj)H(\text{inv.})$ .

The final selection criteria applied in the cutflow tables is the Multivariate selection. To construct this variable, we processed the preselected events through a Boosted Decision Tree (BDT) implemented in XGBOOST [23]. This allows one to construct a single discrimination that can help in separating the signal from background.

The inputs to the Boosted Decision Tree (BDT) consists of a set of kinematic observables. These include the four-momenta of the  $Z$ -boson decay products, the missing four-momentum, transverse missing momentum, missing mass, and the total visible energy in the event. In addition the variables related to the reconstructed Higgs boson such as recoil mass are used. Variables obtained upon reconstructing the  $Z$  boson are also included, such

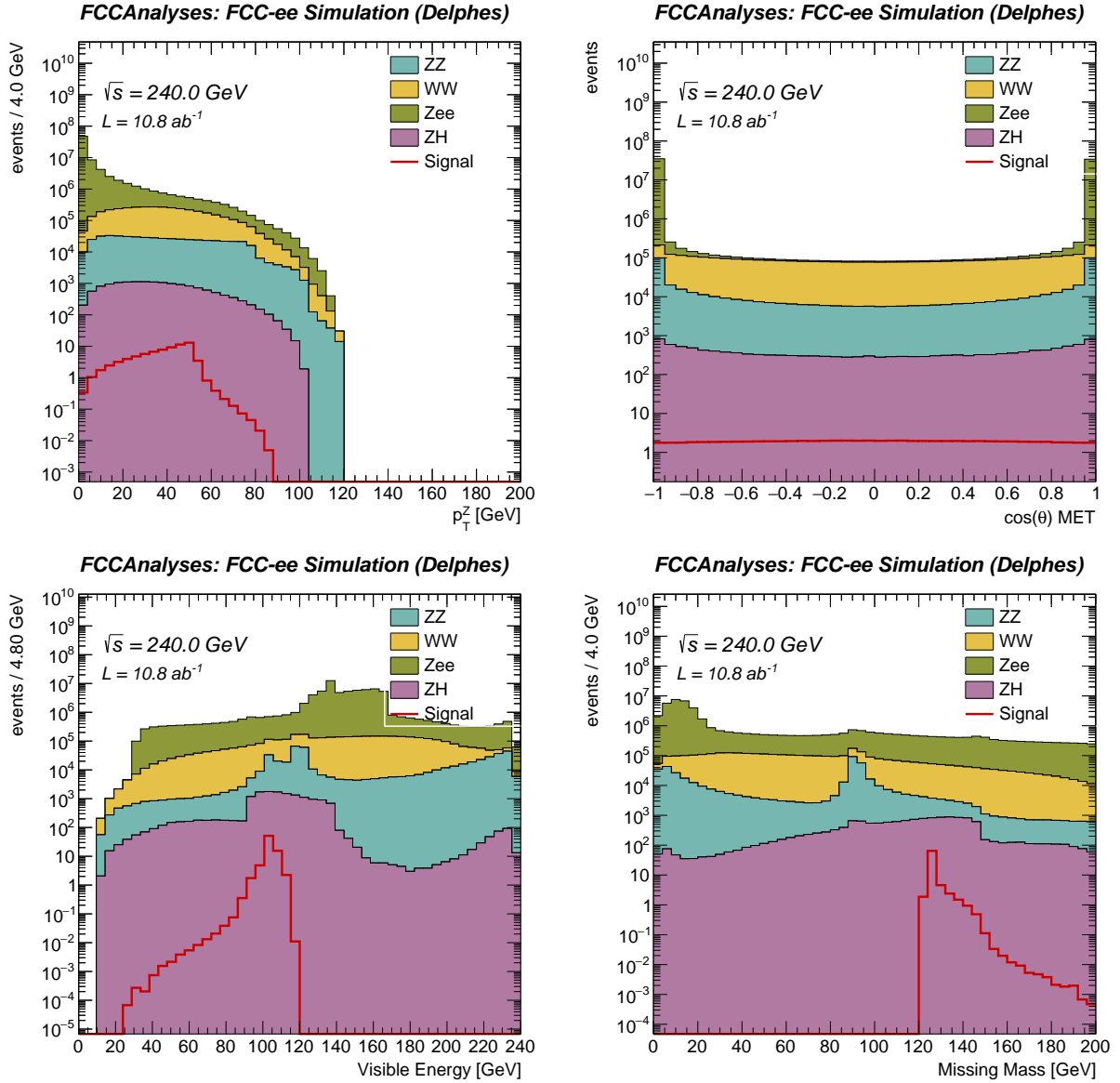


FIG. 1: Kinematic distributions in the  $Z(ee)H(inv.)$  channel after preselection criteria are applied.

as its energy, momentum, and transverse momentum. Moreover, to improve the discriminating power of the BDT, we augment the feature set with variables derived from combinations of the four vector inputs. The momentum imbalance ( $\mathcal{I}_{e_1 e_2}$ ) is defined in the  $Z(ee)H(inv.)$  channel as:

$$\mathcal{I}_{e_1 e_2} = \frac{p_T^{e_1} - p_T^{e_2}}{p_T^{e_1} + p_T^{e_2}} \quad (3)$$

Additionally, we also define the ratios of electron  $p_T$  with the missing  $p_T$  ( $\not{p}_T$ ) as follows:

$$\mathcal{R}_{p_T^{e_1}/\not{p}_T} = \frac{p_T^{e_1}}{\not{p}_T}, \quad (4)$$

$$\mathcal{R}_{p_T^{e_2}/\not{p}_T} = \frac{p_T^{e_2}}{\not{p}_T}. \quad (5)$$

and define the ratio of total electron energy over total electron momenta:

$$\mathcal{R}_{E^e/p^e} = \frac{E^{\text{electron 1}} + E^{\text{electron 2}}}{|\vec{p}^{\text{electron 1}}| + |\vec{p}^{\text{electron 2}}|} \quad (6)$$

Additionally, angular variables between visible objects

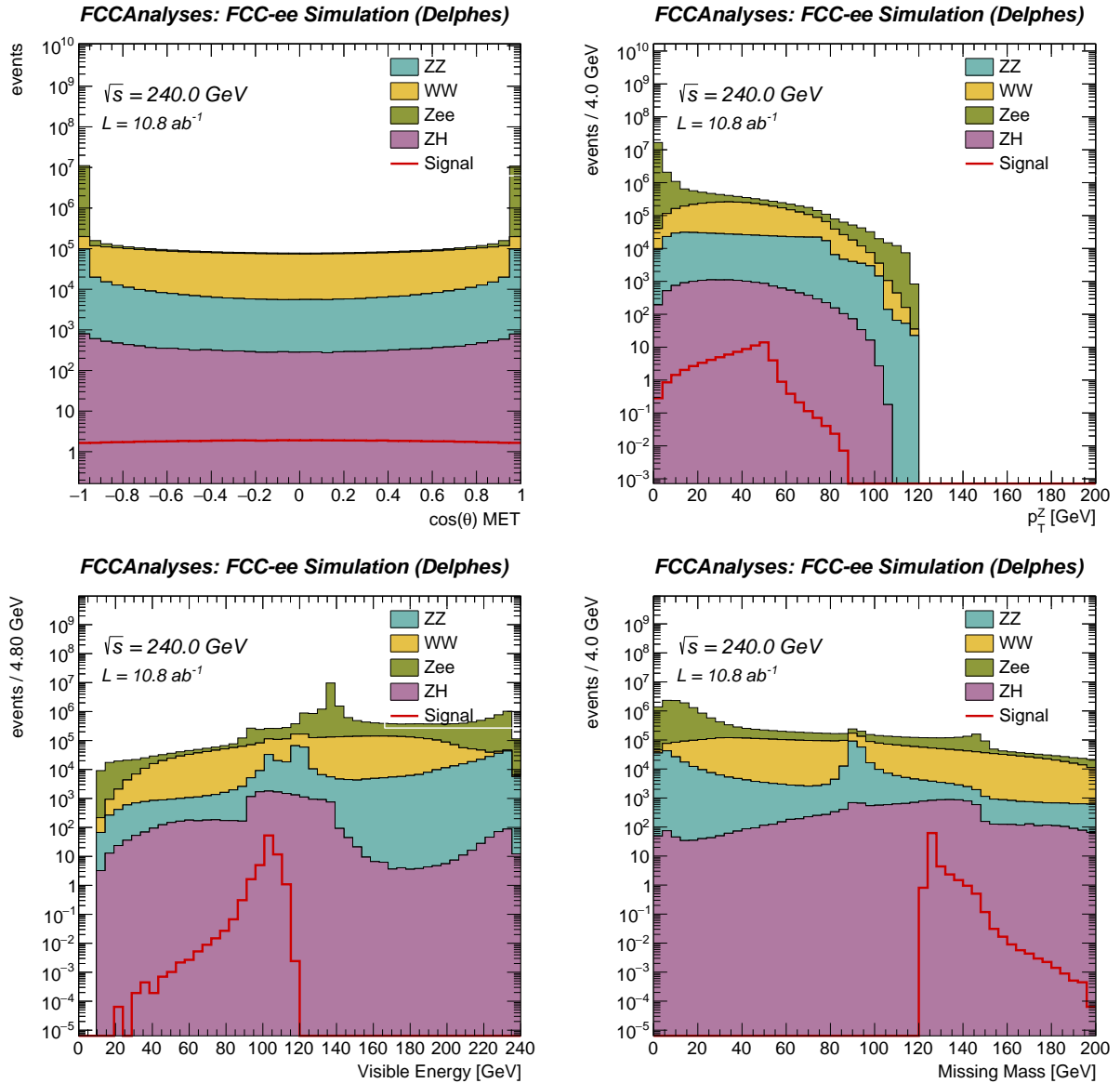


FIG. 2: Kinematic distributions in the  $Z(\mu\mu)H(inv.)$  channel after preselection criteria are applied.

are also used. Similar variables are also defined in the other channels.

The BDT used in this analysis is trained by using the hyperparameter setting as defined in Table VI. The trained BDT model is then converted into ROOT [24] format via CERN ROOT TMVA [25] for a streamlined inference within the FCCANALYSES software. The outcome of this study is a single MVA score that is used to discriminate the signal against the background. The distribution of the MVA score is given in Figure 5a for  $Z(ee)H(inv.)$ , Figure 5b for  $Z(\mu\mu)H(inv.)$ , and Figure 5c for  $Z(jj)H(inv.)$ .

Final selection is then made on the MVA score. We select events with their MVA score greater than 0.95. Thus we see a final significance of  $0.6\sigma$  in both of the leptonic  $Z$  decay channels, i.e., the  $ee$  and  $\mu\mu$  channels, whereas in the hadronic  $Z$  decay channel a significance of  $3.1\sigma$  is achieved.

Based on MVA distribution shown in Figure 5, a reduction in the number of background events is observed in region  $MVA > 0.9$  for the  $Z(jj)H(inv.)$  while no such feature is seen in the  $Z(\ell\ell)H(inv.)$  channels. This behavior may be understood in terms of the relative importance of input variables used in training the BDT models for

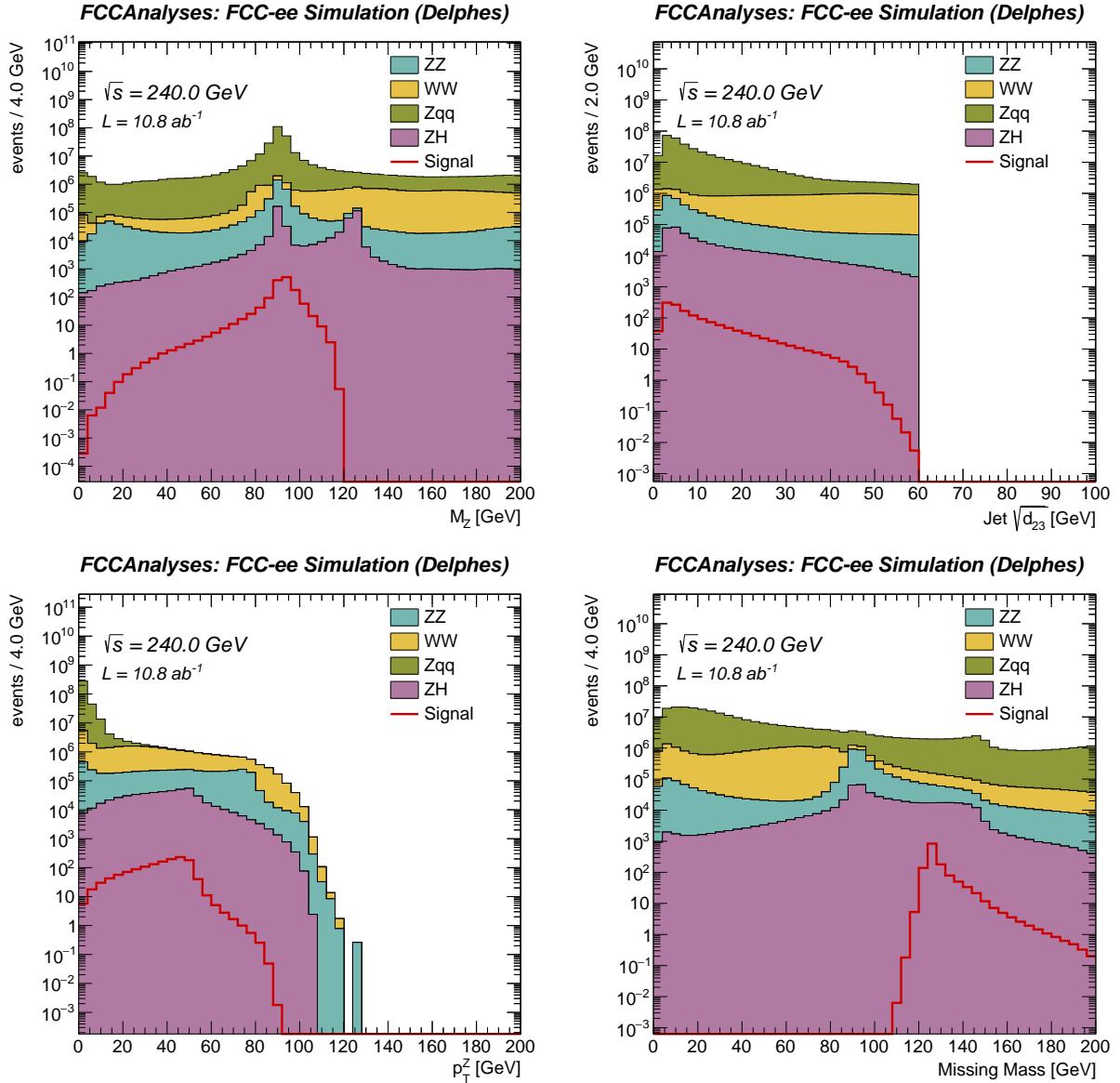


FIG. 3: Kinematic distributions in the  $Z(jj)H(inv.)$  channel after preselection criteria are applied.

the three channels, as given in Figure 4. Accordingly, it is found that the leptonic channels rank the  $p_T^Z$ ,  $\cos(\theta_{\text{miss}})$  and  $E^{\text{vis}}$  as the top three important variables whereas in the hadronic channel, the  $M_Z$ ,  $d_{23}$  and  $p_T^Z$  ranked as the highest three variables based on their importance. The corresponding kinematic distributions are presented in Figure 1, Figure 2, and Figure 3. We note that  $p_T^Z$  is among the most important variables across all channels. However, the  $\cos(\theta_{\text{miss}})$  distribution which is ranked highest by the leptonic channel has a relatively flat shape which leads weaker discriminating power compared with the  $d_{23}$  distribution in  $Z(jj)H(inv.)$  channel. This ef-

fect combined with the larger branching fraction of the  $Z$  boson decay to hadrons ( $\mathcal{B}(Z \rightarrow \text{hadronic}) \sim 69\%$ ) compared with  $\mathcal{B}(Z \rightarrow \mu\mu/ee) \sim 3.4\%$  leads to higher sensitivity in the  $Z(jj)H(inv.)$  channel compared to the  $Z(\ell\ell)H(inv.)$  channels.

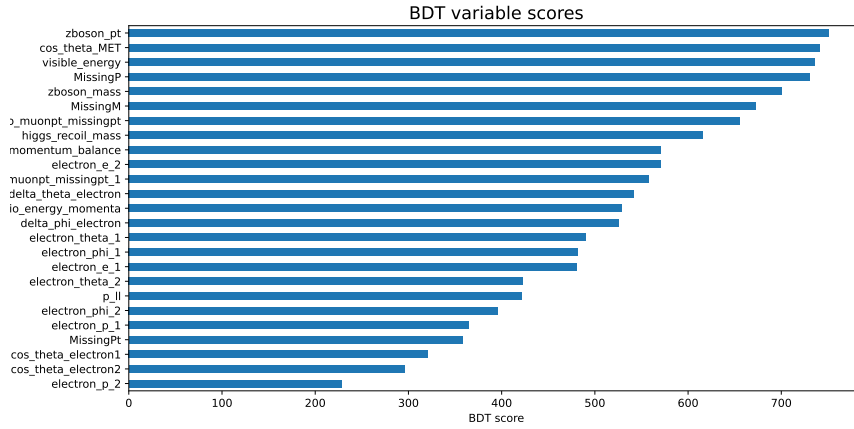
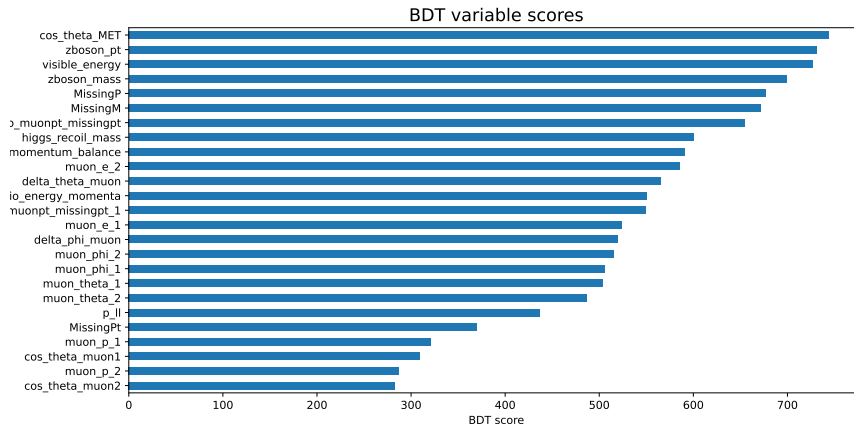
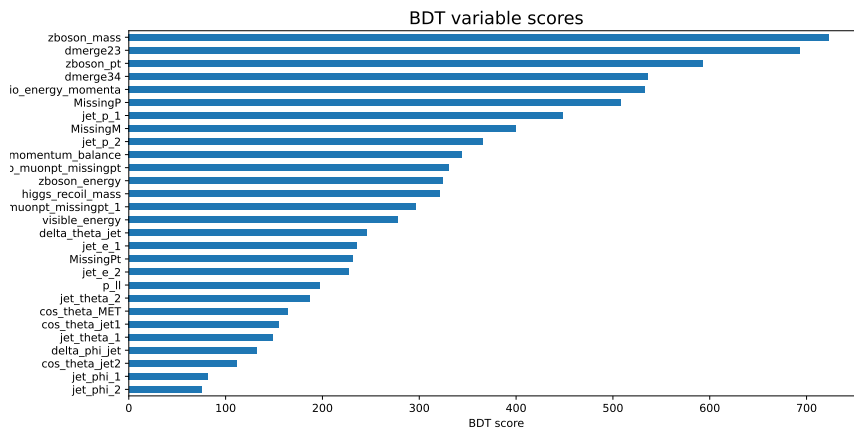
(a)  $ee$  channel(b)  $\mu\mu$  channel(c)  $qq$  channelFIG. 4: Ranking of input variables by their importance in the BDT for the  $ee$ ,  $\mu\mu$ , and  $qq$  channels.

TABLE III: Cut-flow table for the  $Z(ee)H(\text{inv})$  channel showing signal ( $S$ ), background contributions, total background, and statistical significance.

Selection	$S$	$ZZ$	$WW$	$Zee$	$ZH$ (bkg)	$B_{\text{tot}}$	$Z = \frac{S}{\sqrt{S+B}}$
Preselection	76	$5.08 \times 10^5$	$3.32 \times 10^6$	$7.04 \times 10^7$	$1.53 \times 10^4$	$7.42 \times 10^7$	0.01
$87 < m_Z < 95$ GeV	51	$1.95 \times 10^5$	$1.29 \times 10^5$	$1.11 \times 10^7$	$9.73 \times 10^3$	$1.15 \times 10^7$	0.02
$120 < m_{\text{recoil}} < 130$ GeV	42	$1.22 \times 10^4$	$1.95 \times 10^4$	$3.00 \times 10^5$	$1.71 \times 10^3$	$3.34 \times 10^5$	0.07
$ \cos \theta_{\text{miss}}  < 0.80$	34	$3.34 \times 10^3$	$1.46 \times 10^4$	12	$1.22 \times 10^3$	$1.91 \times 10^4$	0.24
Ratio $p_T^e/p_T^{\text{miss}} < 2.0$	34	$2.84 \times 10^3$	$1.43 \times 10^4$	0	$1.16 \times 10^3$	$1.83 \times 10^4$	0.25
$120 < m_{\text{miss}} < 140$ GeV	34	$1.69 \times 10^3$	$9.04 \times 10^3$	0	$9.78 \times 10^2$	$1.17 \times 10^4$	0.31
MVA $> 0.95$	29	388	$1.82 \times 10^3$	0	216	$2.42 \times 10^3$	0.59

TABLE IV: Cut-flow table for the  $Z(\mu\mu)H(\text{inv})$  channel showing signal ( $S$ ), background contributions, total background, and statistical significance.

Selection	$S$	$ZZ$	$WW$	$Z\mu\mu$	$ZH$ (bkg)	$B_{\text{tot}}$	$Z = \frac{S}{\sqrt{S+B}}$
Preselection	73	$5.01 \times 10^5$	$3.17 \times 10^6$	$2.21 \times 10^7$	$1.53 \times 10^4$	$2.58 \times 10^7$	0.01
$87 < m_Z < 95$ GeV	55	$2.13 \times 10^5$	$1.25 \times 10^5$	$1.03 \times 10^7$	$1.08 \times 10^4$	$1.07 \times 10^7$	0.02
$120 < m_{\text{recoil}} < 130$ GeV	46	$1.30 \times 10^4$	$1.83 \times 10^4$	$1.63 \times 10^5$	$1.92 \times 10^3$	$1.97 \times 10^5$	0.10
$ \cos \theta_{\text{miss}}  < 0.80$	38	$3.53 \times 10^3$	$1.36 \times 10^4$	0	$1.39 \times 10^3$	$1.85 \times 10^4$	0.27
Ratio $p_T^\mu/p_T^{\text{miss}} < 2.0$	38	$3.00 \times 10^3$	$1.34 \times 10^4$	0	$1.31 \times 10^3$	$1.77 \times 10^4$	0.28
$120 < m_{\text{miss}} < 140$ GeV	38	$1.90 \times 10^3$	$9.62 \times 10^3$	0	$1.14 \times 10^3$	$1.27 \times 10^4$	0.33
MVA $> 0.95$	33	402	$1.87 \times 10^3$	0	234	$2.51 \times 10^3$	0.65

TABLE V: Cut-flow table for the  $Z(jj)H(\text{inv})$  channel showing signal ( $S$ ), background contributions, total background, and statistical significance.

Selection	$S$	$ZZ$	$WW$	$Zqq$	$ZH$ (bkg)	$B_{\text{tot}}$	$Z = \frac{S}{\sqrt{S+B}}$
Preselection	$1.39 \times 10^3$	$4.15 \times 10^6$	$2.39 \times 10^7$	$3.35 \times 10^8$	$5.14 \times 10^5$	$3.64 \times 10^8$	0.07
$87 < m_Z < 95$ GeV	850	$1.93 \times 10^6$	$1.04 \times 10^6$	$1.64 \times 10^8$	$1.98 \times 10^5$	$1.68 \times 10^8$	0.06
$120 < m_{\text{recoil}} < 130$ GeV	702	$5.46 \times 10^4$	$3.77 \times 10^4$	$1.75 \times 10^6$	$3.26 \times 10^4$	$1.88 \times 10^6$	0.51
$ \cos \theta_{\text{miss}}  < 0.80$	574	$3.86 \times 10^4$	$2.56 \times 10^4$	288	$2.37 \times 10^4$	$8.82 \times 10^4$	1.93
MVA $> 0.95$	341	$5.93 \times 10^3$	$2.52 \times 10^3$	57	$2.89 \times 10^3$	$1.14 \times 10^4$	3.14

TABLE VI: XGBoost hyperparameters used in the BDT training.

Parameter	Value	Parameter	Value
Objective	binary:logistic	Eval metric	logloss
Max depth	6	Subsample	0.5
Colsample by tree	0.5	Tree method	hist
Number of estimators	500	Early stopping rounds	30
Learning rate	0.15	Gamma	3
Min child weight	10	Max delta step	0

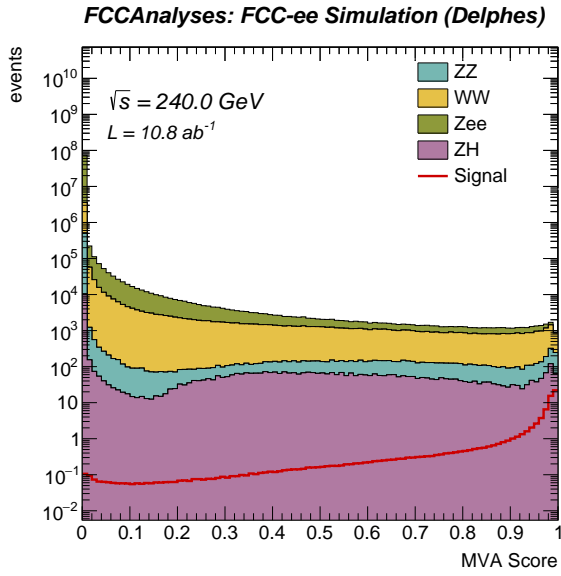
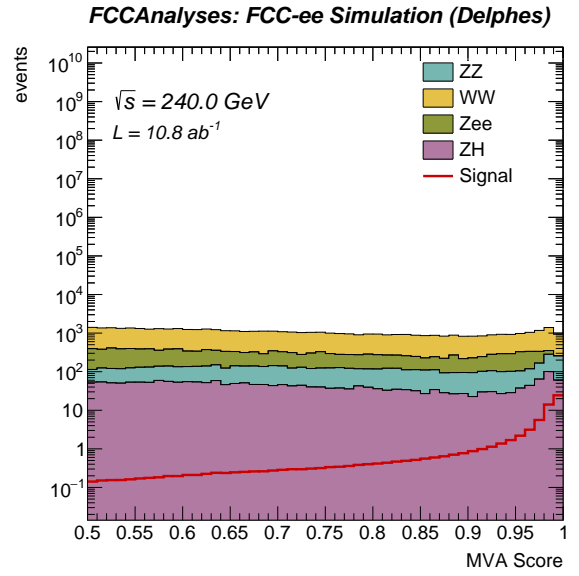
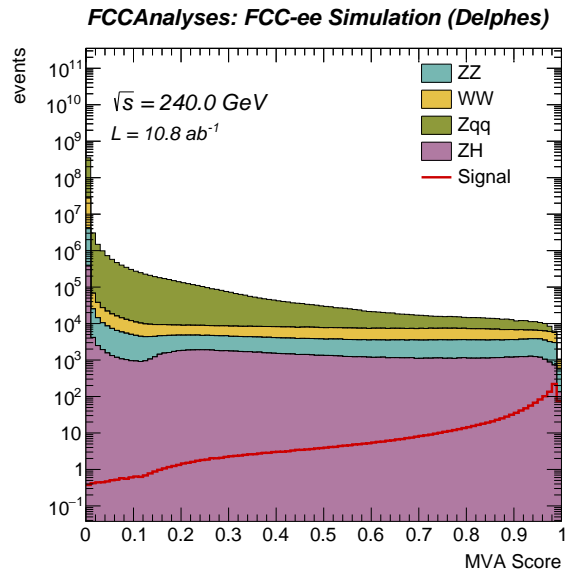
(a)  $ee$  channel(b)  $\mu\mu$  channel(c)  $qq$  channelFIG. 5: MVA score after preselection criteria for the  $ee$ ,  $\mu\mu$ , and  $qq$  channels.

TABLE VII: Expected 95% CL upper limits on the branching fraction for the  $ee$ ,  $\mu\mu$ , and  $qq$  channels.

Physics	Upper Limit on $\mathcal{B}(H \rightarrow inv.)$
$Z(ee)H(inv)$	0.43%
$Z(\mu\mu)H(inv)$	0.35%
$Z(qq)H(inv)$	0.15%
<b>Combined</b>	<b>0.15%</b>

#### IV. STATISTICAL ANALYSIS

As the significance of  $5\sigma$  is not achieved in any of the channels we derive the upper limits on the  $\mathcal{B}(H \rightarrow inv.)$ . The statistical analysis to evaluate the upper limits is performed using the CMS COMBINE software [26]. We use the missing mass  $M_{\text{miss}}$  as an input variable for statistical analysis. The pseudo-data is obtained by combining the signal and background distributions after scaling these with their corresponding cross-section and luminosity. A normalisation uncertainty of 10% is assigned for the modeling of background processes. The luminosity is assigned an uncertainty of 1%. The CMS COMBINE software’s implementation of the `AsymptoticLimits` function which is based on Ref. [27] is used to obtain the limits. We find the following 95% confidence level upper

limits on  $\mathcal{B}(H \rightarrow inv.)$ : 0.43% in the  $Z \rightarrow ee$  channel; 0.35% in the  $Z \rightarrow \mu\mu$  channel and 0.15% in the  $Z \rightarrow jj$  channel. The combined upper limit at 95% C.L. is found as 0.15%. A summary of the results is given in Table VII.

#### V. CONCLUSIONS

In this work, we studied the invisible decays of Higgs boson in the  $ZH$  process at the FCCee at  $\sqrt{s} = 240$  GeV. We analyzed the invisible Higgs boson decay in the three different physics processes:  $Z(\rightarrow ee)H(\rightarrow inv)$ ,  $Z(\rightarrow \mu\mu)H(\rightarrow inv)$ , and the  $Z(\rightarrow jj)H(\rightarrow inv)$  channels. The  $Z \rightarrow jj$  channel in this analysis consists of  $Z \rightarrow bb$ ,  $Z \rightarrow cc$ ,  $Z \rightarrow ss$  and  $Z \rightarrow qq$  channels which are combined with appropriate weighting with respect to their branching fraction. We find upper limits on the  $\mathcal{B}(H \rightarrow inv.)$ . Among the three channels, we note that the hadronic channel owing to its higher event yield ( $\mathcal{B}(Z \rightarrow \text{hadronic}) \sim 69\%$  versus  $\mathcal{B}(Z \rightarrow \mu\mu/ee) \sim 3.4\%$ ), has higher sensitivity in deriving the upper limit for the  $H(\rightarrow inv)$  process. A combined upper limit 95% C.L. on the  $\mathcal{B}(H \rightarrow inv.)$  for three channels is found as 0.15%.

- 
- [1] LHC HIGGS CROSS SECTION WORKING GROUP collaboration, D. de Florian et al., *Handbook of LHC Higgs Cross Sections: 4. Deciphering the Nature of the Higgs Sector*, *CERN Yellow Rep. Monogr.* **2** (2017) 1–869, [1610.07922].
- [2] ATLAS collaboration, G. Aad et al., *Combination of searches for invisible decays of the Higgs boson using 139 fb<sup>-1</sup> of proton-proton collision data at  $s=13$  TeV collected with the ATLAS experiment*, *Phys. Lett. B* **842** (2023) 137963, [2301.10731].
- [3] CMS collaboration, A. Tumasyan et al., *A search for decays of the Higgs boson to invisible particles in events with a top-antitop quark pair or a vector boson in proton-proton collisions at  $\sqrt{s} = 13$  TeV*, *Eur. Phys. J. C* **83** (2023) 933, [2303.01214].
- [4] FCC collaboration, M. Benedikt et al., *Future Circular Collider Feasibility Study Report: Volume 1, Physics, Experiments, Detectors*, 4, 2025.
- [5] M. Selvaggi, J. Eysermans and A. Blondel, *Prospects in Electroweak, Higgs and Top physics at FCC*, Mar., 2025. 10.17181/n2emg-43f06.
- [6] Y. Tan et al., *Search for invisible decays of the Higgs boson produced at the CEPC*, *Chin. Phys. C* **44** (2020) 123001, [2001.05912].
- [7] CLICDP collaboration, K. Mekala, A. F. Zarnecki, B. Grzadkowski and M. Iglicki, *Sensitivity to invisible scalar decays at CLIC*, *Eur. Phys. J. Plus* **136** (2021) 160, [2002.06034].
- [8] A. Ishikawa, *Search for invisible decays of the Higgs boson at the ILC*, *PoS LeptonPhoton2019* (2019) 147, [1909.07537].
- [9] A. Mehta, N. Rompotis and S. Randles, *Higgs to invisible at the fcc-ee*, Mar., 2025. 10.17181/9b128-qqc43.
- [10] FCC Collaboration, “IDEA—FCC-ee Winter 2023 Monte-Carlo Production.” <https://fcc-physics-events.web.cern.ch/fcc-ee/rec/winter2023/IDEA>, 2023.
- [11] W. Kilian, T. Ohl and J. Reuter, *WHIZARD: Simulating Multi-Particle Processes at LHC and ILC*,

- Eur. Phys. J. C* **71** (2011) 1742, [0708.4233].
- [12] T. Sjöstrand, S. Mrenna and P. Z. Skands, *PYTHIA 6.4 Physics and Manual*, *JHEP* **05** (2006) 026, [hep-ph/0603175].
- [13] T. Sjöstrand, S. Ask, J. R. Christiansen, R. Corke, N. Desai, P. Ilten et al., *An introduction to PYTHIA 8.2*, *Comput. Phys. Commun.* **191** (2015) 159–177, [1410.3012].
- [14] IDEA STUDY GROUP collaboration, M. Abbrescia et al., *The IDEA detector concept for FCC-ee*, February, 2025.
- [15] DELPHES 3 collaboration, J. de Favereau, C. Delaere, P. Demin, A. Giammanco, V. Lemaître, A. Mertens et al., *DELPHES 3, A modular framework for fast simulation of a generic collider experiment*, *JHEP* **02** (2014) 057, [1307.6346].
- [16] S. D. Ellis and D. E. Soper, *Successive Combination Jet Algorithm for Hadron Collisions*, *Phys. Rev. D* **48** (1993) 3160–3166, [hep-ph/9305266].
- [17] S. Catani, Y. L. Dokshitzer, M. Olsson, G. Turnock and B. R. Webber, *New Clustering Algorithm for Multi-Jet Cross-Sections in  $e^+e^-$  Annihilation*, *Phys. Lett. B* **269** (1991) 432–438.
- [18] S. Catani, Y. L. Dokshitzer, M. H. Seymour and B. R. Webber, *Longitudinally Invariant  $k_t$  Clustering Algorithms for Hadron–Hadron Collisions*, *Nucl. Phys. B* **406** (1993) 187–224.
- [19] M. Cacciari, G. P. Salam and G. Soyez, *FastJet User Manual*, *Eur. Phys. J. C* **72** (2012) 1896, [1111.6097].
- [20] G. Salam, “Basic Guidance on Jet Algorithms (and FastJet) for FCC-ee.” Presentation at the FCC Physics Performance Meeting, 2022.
- [21] KEY4HEP collaboration, A. Sailer et al., *The Key4hep software stack: Beyond Future Higgs factories*, December, 2023. 2312.08151.
- [22] C. Helsen, E. Perez, M. Selvaggi, V. Volkl, L. Forthomme and J. Munch Torndal, *HEP-FCC/FCCAnalyses: v0.11.0*, May, 2025. 10.5281/zenodo.15528870.
- [23] T. Chen and C. Guestrin, *XGBoost: A Scalable Tree Boosting System*, in *Proceedings of the 22nd ACM SIGKDD International Conference on Knowledge Discovery and Data Mining*, pp. 785–794, ACM, 2016. 1603.02754. DOI.
- [24] R. Brun and F. Rademakers, *ROOT — An Object Oriented Data Analysis Framework*, *Nucl. Instrum. Meth. A* **389** (1997) 81–86.
- [25] H. Voss, A. Hocker, J. Stelzer and F. Tegenfeldt, *TMVA, the Toolkit for Multivariate Data Analysis with ROOT*, *PoS ACAT* (2007) 040.
- [26] CMS collaboration, A. Hayrapetyan et al., *The CMS Statistical Analysis and Combination Tool: Combine*, *Comput. Softw. Big Sci.* **8** (2024) 19, [2404.06614].
- [27] G. Cowan, K. Cranmer, E. Gross and O. Vitells, *Asymptotic formulae for likelihood-based tests of new physics*, *Eur. Phys. J. C* **71** (2011) 1554, [1007.1727].